Host infection selects for sRNA variants that drive bacterial social cheating

Running title: ArcZ mutations drive bacterial cheating

Authors: **Quentin Dubois[1], Typhaine Brual[1], Véronique Utzinger[1], Romain Mercier[2], Jérémy Cigna[3], Agnès Rodrigue[1], Laetitia Attaiech[4], Erwan Gueguen[1]***

Affiliation:
[1] Université Claude Bernard Lyon1, CNRS, INSA Lyon, UMR5240 MAP, F-69622, LYON, France.
[2] Molecular Microbiology and Structural Biochemistry (MMSB), Université Claude Bernard Lyon 1, CNRS, Inserm, UMR5086, 69007 Lyon, France.
[3] French Federation of Seed Potato Growers (FN3PT-inov3PT), 43-45 rue de Naples, 75008 Paris, France.
[4] CIRI, Centre International de Recherche en Infectiologie, Team "Horizontal gene transfer in bacterial pathogens" (Horigene), Inserm, U1111, Université Claude Bernard Lyon 1, CNRS, UMR5308, Ecole Normale Supérieure de Lyon, 69007, Lyon, France.

*Corresponding author: erwan.gueguen@univ-lyon1.fr

Orcid I.D.

G.E.	0000-0001-8784-1491
A.L.	0000-0002-6188-1839
C.J.	0000-0002-1219-7096
B.T	0000-0001-5179-8882
M.R.	0000-0002-6170-4322
R.A.	0000-0002-8473-8103
D.Q.	0009-0009-4917-8495
U.V.	0009-0008-4634-7188

Key words: *Dickeya solani*, secondary metabolites, oocydin, zeamine, solanimycin, bacteria, yeast, fungi, ascomyceta, sRNA, ArcZ, SNP, Nucleotide Variations, Experimental Inconsistencies, Type Strain IPO 2222, Plant Pathogen, Genetic Diversity, Phenotypic Variation, Cheating, Hfq

Abstract

Intra-strain variation in model bacterial pathogens can compromise experimental reproducibility and obscure biological interpretations. *Dickeya solani*, a necrotrophic potato pathogen, is widely studied using the type strain IPO 2222. However, phenotypic discrepancies among laboratories led us to investigate the genetic integrity of this reference stock. We identified at least three distinct IPO 2222 variants co-existing in the original stock, differing solely by mutations in the gene encoding the small regulatory RNA (sRNA) ArcZ. These findings resolve conflicting reports of antimicrobial activity in this strain described by Brual *et al*. (PLOS Genetics 19, e1010725, 2023) and Matilla *et al*. (mBio, e02472-22, 2022).

We demonstrate that these are adaptive mutations rapidly selected *in planta* during host infection. Crucially, rather than systematically inactivating the gene, these mutations modulate the cellular levels of processed ArcZ. This modulation can uncouple virulence from antimicrobial activity. These variants behave as social cheaters, exhibiting a frequency-dependent fitness advantage over the cooperative wild-type strain during co-infection.

These findings provide evidence that remodeling of a pleiotropic sRNA drives the emergence of bacterial cheaters within a plant host. The speed at which these mutants sweep through the population underscores the intense selective pressure acting on regulatory networks during infection, identifying sRNA modulation as a pivotal mechanism for rapid short-term adaptation.

Significance Statement

Bacterial pathogens often utilize cooperative behaviors, such as the secretion of communal "public goods," to colonize hosts. We demonstrate that the plant pathogen *Dickeya solani* rapidly evolves "cheater" variants during infection through single-nucleotide mutations in the small regulatory RNA (sRNA) ArcZ. These mutations, concentrated within a 150-nucleotide region, modulate sRNA levels to uncouple virulence from antimicrobial production. This trade-off provides a significant fitness advantage during co-infection, revealing an evolutionarily accessible mechanism for social cheating. Our work highlights how minute noncoding elements serve as critical targets of selection, shaping both pathogenesis and microbial social dynamics.

Introduction

In microbial communities, cooperative traits such as quorum sensing, public goods secretion, and virulence factor production impose significant metabolic costs. This cooperation creates a selective pressure for the emergence of "cheaters". These variants benefit from communal goods without bearing the costs of their production and often gain a competitive advantage over their cooperative counterparts. Such behavior influences pathogenic interaction dynamics in both animal and plant systems (1–3). The emergence of cheating is frequently driven by point mutations in protein-coding genes that regulate virulence (3). For instance, siderophore-negative *Pseudomonas aeruginosa* strains persist by utilizing iron-chelating molecules secreted by others, while Type III secretion system-negative mutants can outcompete producers during infection (2, 4, 5).

Dickeya solani, a pectinolytic bacterium of the *Pectobacteriaceae* family, serves as a valuable model for studying these dynamics in phytopathology. This pathogen causes severe soft rot in potato plants (6, 7). Since its emergence in Europe, this species has been prioritized as one of the top ten bacterial pathogens of concern in agriculture (8). *D. solani, as other pectinolytic bacteria species,* is characterized by an aggressive infection phenotype that causes stem rotting, leaf wilt, and desiccation (9). Its pathogenicity relies on the secretion of a broad spectrum of plant-cell-wall-degrading enzymes (PCWDEs), including pectinases, cellulases, and proteases, which macerate host tissues to release nutrients (10). In addition to these virulence factors, *D. solani* invests in the production of diverse secondary metabolites, such as the antiascomyceta solanimycin, the phytotoxic zeamine, and the antioomyceta oocydin (11).

The regulation of these traits relies centrally on ArcZ, a highly conserved, Hfq-dependent small sRNA (12, 13). To exert its regulatory activity, the primary ArcZ transcript undergoes specific processing by the endonuclease RNase E, releasing a functional short isoform derived from its 3' end (14). This mature form acts as a global pleiotropic regulator, controlling the expression of more than 10% of the bacterial

genome, including master regulators of the general stress response (*rpoS*) (15) and motility (*flhDC*) (16). In the model phytopathogen *Dickeya dadantii* 3937, ArcZ has been identified as a key virulence activator. It promotes the production of plant cell wall-degrading enzymes by binding directly to the 5'-untranslated region (5' UTR) of the *pecT* mRNA, thereby relieving the repression exerted by this transcriptional regulator (17). ArcZ is known to control the synthesis of antimicrobial secondary metabolites in the closely related species *D. solani* (11). However, to date, no specific mRNA target has been identified or confirmed in this species .

The type strain IPO 2222, isolated from a potato plant in a crop field in the Netherlands in 2007, serves as a foundational model for this species in numerous studies (18–25). However, its phenotypic stability has been the subject of conflicting reports (11, 25). While our past study described the strain as lacking antimicrobial activity due to a mutation in the *arcZ* gene (11), others have observed robust anti-yeast activity in the same strain (25). In this study, we investigated the genetic basis of these discrepancies and found that they arise from unrecognized population heterogeneity within the original cryotube stored in The Netherlands.

We identified multiple *IPO 2222* variants co-existing in the original stock, distinct solely by mutations in the gene encoding the sRNA ArcZ. We demonstrate here that these are adaptive mutations rapidly selected *in planta* during host infection. Crucially, these mutations modulate the cellular levels of processed ArcZ rather than strictly inactivating the gene. This modulation uncouples virulence from antimicrobial activity, allowing these variants to behave as social cheaters that exhibit a frequency-dependent fitness advantage over the cooperative wild-type strain. These findings provide evidence that remodeling a pleiotropic sRNA drives the emergence of bacterial cheaters within a plant host, identifying sRNA modulation as a pivotal mechanism for rapid short-term adaptation.

Results

Phenotypic and genotypic heterogeneity of *D. solani* IPO 2222 in laboratory stocks

The *Dickeya solani* type strain, IPO 2222, was originally isolated from a diseased potato plant in the Netherlands. Following its sequencing, this strain was distributed to numerous culture collections (e.g., NCPPB, BCCM) and research laboratories across Europe. The genomic sequence of IPO 2222 (NCBI accession NZ_CP015137.1) contains a G90A mutation in the *arcZ* gene, designated as the $arcZ_2$ allele. We previously demonstrated that this mutation impairs the processing of the ArcZ sRNA, resulting in a loss of solanimycin production and antifungal activity, a phenotype we define here as Sol^- (11).
While our laboratory strain (DS45; **table S1 and S3**) and the reference genome NZ_CP015137.1 carry the $arcZ_2$ allele, a conflicting report has described IPO 2222 as capable of inhibiting yeast growth (25). To resolve this discrepancy, we analyzed IPO 2222 isolates from various European sources **(Fig. 1A)**. Phenotypic screening revealed that strains obtained from Paris (FR) (DS45), the BCCM in Belgium (BE) (DS486), the NCPPB in United Kingdom (UK) (DS566), and Gdansk (PL) (DS470) were unable to inhibit *Kluyveromyces lactis* growth. Whereas strain D s0432-1 (FR) (DS49), with $arcZ_1$ allele, is able to inhibit *K. lactis* growth (**Fig. 1A and Fig. S1A**). Genomic sequencing confirmed that these Sol^- isolates share the $arcZ_2$ genotype found in the reference genome (**table S1**). In contrast, the isolate obtained from the James Hutton Institute in Scotland (DS620) exhibited antifungal activity (**Fig. 1A and Fig. S1A**). Sequencing of DS620 revealed a distinct genotype carrying a specific G101T mutation, yielding the $arcZ_3$ allele (**table S1**).
This genetic divergence is reflected in public databases, where IPO 2222 has been sequenced at two distinct time points. In 2013, the James Hutton Institute deposited a genome assembly (GenBank accession CM001859.1), while in 2016, the Institute for Integrative Biology of the Cell in France deposited the current reference. Our analysis of the *arcZ* locus in these two available genomes confirms the presence of the G101T mutation in the Scottish sequence and the G90A mutation in the French sequence (NZ_CP015137.1). These public data provide historical evidence that two distinct *arcZ* alleles already existed within the IPO 2222 lineage.
We hypothesized that this diversity originated from the initial stock. We analyzed a spread plate prepared from an aliquot of the original IPO 2222 cryotube sent directly by J. Van der Wolf's laboratory from Wageningen University (The Netherlands). Of 925 colonies screened, the majority (94%) were

Sol$^-$, while a minority displayed antifungal activity against *K. lactis* (not shown). The active strain variants presented two distinct phenotypes: wide inhibition halos (exemplified by isolate DS624) and intermediate halos (exemplified by isolate DS625) (**Fig. 1B & table 2**). Whole-genome and Sanger sequencing of these multiple IPO 2222 sub-isolates resolved the genetic basis of this heterogeneity. The Sol$^-$ isolate, designated as DS623, carries the *arcZ*$_2$ allele and is genomically identical to the NCBI reference. Conversely, the isolate exhibiting a wide inhibition halo (DS624) carries the wild-type *arcZ*$_1$ allele, resulting from an A90G reversion relative to the reference, which restores full antifungal activity. Finally, the isolate displaying an intermediate halo (DS625) is identical to the Scottish strain DS620 and carries the *arcZ*$_3$ allele characterized by the G101T mutation (**table 2**). To further characterize the genomic diversity of the initial stock, we performed Illumina deep sequencing directly on DNA extracted from the original cryotube content (**Fig. 1C**). This analysis confirmed the distribution of variants: the *arcZ*$_2$ (G90A) mutant represented 93% of the sequenced reads, whereas the *arcZ*$_3$ (G101T) variant and the wild-type *arcZ*$_1$ allele accounted for 4% and 2% of the reads, respectively.
These data demonstrate that the original cryopreserved stock of *D. solani* IPO 2222 is not clonal but consists of at least three coexisting variants carrying the *arcZ*$_1$, *arcZ*$_2$ or *arcZ*$_3$. This heterogeneity likely explains the conflicting phenotypic descriptions of IPO 2222 in the literature. Crucially, the detection of these minor allelic variants (*arcZ*$_1$ and *arcZ*$_3$) by deep sequencing was not merely a computational observation but was independently validated by the physical isolation of viable colonies from the same original stock. These isolates, which exhibited the predicted phenotypes, were confirmed by targeted Sanger sequencing to carry the exact mutations identified in the NGS population analysis, thereby ruling out sequencing or mapping artifacts.

Virulence and antimicrobial production display distinct sensitivities to ArcZ dosage.

ArcZ is a highly conserved regulatory sRNA with pleiotropic functions. ArcZ is known to positively regulate virulence in *D. dadantii* (17), in addition to its role in solanimycin production in *D. solani*. While the *arcZ*$_2$ allele is known to abolish antifungal activity, its impact on *D. solani* pathogenicity remained unclear. We assessed the virulence of the identified coexisting variants using a potato tuber maceration assay (**Fig. 1D**). Strains carrying the wild-type *arcZ*$_1$ allele induced extensive tissue maceration. In contrast, the *arcZ*$_2$ variant (DS623) exhibited significantly reduced virulence. Surprisingly, the *arcZ*$_3$ variant (DS625), which displayed only intermediate antifungal activity, retained full pathogenic potential comparable to the wild-type strain (**Fig. 1D**).
To ensure these results were broadly representative, we extended our analysis to a panel of *D. solani* isolates from diverse European collections (**Fig. 1A, S1B**). This broader analysis consistently supported the results of the cryotube variants: all tested *arcZ*$_2$ strains from diverse collections displayed a uniform reduction in virulence, whereas the *arcZ*$_3$ strain (from the Scottish collection) maintained full virulence.
To elucidate the molecular basis of these phenotypic differences, we analyzed ArcZ expression and processing by Northern blot (**Fig. 1E**). As anticipated, the *arcZ*$_2$ strain failed to accumulate the functional form of ArcZ, i.e. the processed sRNA form. The wild-type *arcZ*$_1$ strain showed high levels of the processed transcript, while the *arcZ*$_3$ variant accumulated the processed form at visibly reduced levels. This molecular pattern was confirmed across the European isolates, where *arcZ*$_2$ isolates lacked the processed form and the *arcZ*$_3$ strain showed intermediate levels (**Fig. S1C**).
Collectively, these data suggest that solanimycin production and pathogenicity are controlled by differential sensitivities to ArcZ concentration. The intermediate accumulation of ArcZ in the *arcZ*$_3$ variant correlates with its reduced antifungal activity but is clearly sufficient to support full virulence. Therefore, solanimycin biosynthesis appears to require a high threshold of ArcZ, whereas virulence functions are maintained even at lower intracellular ArcZ levels.

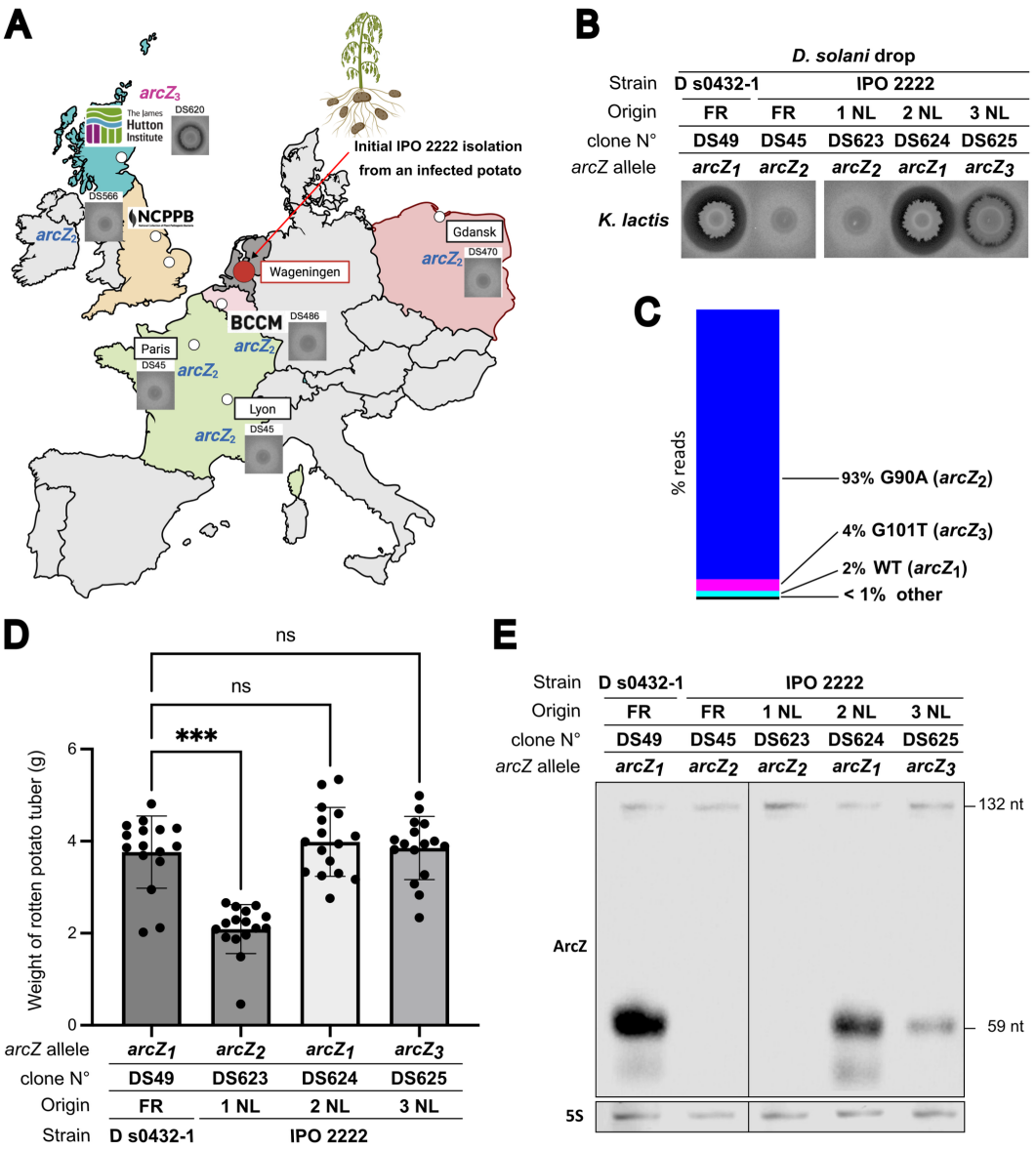

Figure 1. Geographic and genotypic heterogeneity of *Dickeya solani* isolates across Europe. (A) Geographic distribution of *D. solani* strains obtained from European collections. Insets display representative antifungal inhibition halos for isolates from each location. Two *arcZ* allelic variants ($arcZ_2$ and $arcZ_3$) were identified in addition to the wild type. The map was created with Biorender. **(B)** Antifungal activity against *Kluyveromyces lactis*. Representative halos are shown for *D. solani* strain D s0432-1 and three IPO 2222 sub-isolates (1, 2, and 3) recovered from the cryotube of the reference strain IPO 2222 in The Netherlands (7). Drops of bacterial culture were spotted on yeast-containing agar plates and incubated for 48 h at 30 °C. Four replicates were performed for this experiment. **(C)** Deep sequencing analysis of the *arcZ* locus in the IPO 2222 reference stock. The relative frequency of the wild-type ($arcZ_1$) and mutant alleles (G90A/$arcZ_2$ and G101T/$arcZ_3$) indicates strain heterogeneity. Two replicates were performed for this experiment. **(D)** Virulence assay on potato tubers. Maceration was quantified by weighing rotten tissue 48 h post-infection. The $arcZ_2$ variant exhibits significantly reduced virulence compared to the $arcZ_1$ and $arcZ_3$ variants. Data are presented as mean ± SD; *** $p < 0.001$, ns: not significant. 16 replicates were performed for this experiment. **(E)** Northern blot analysis of *arcZ* expression. A probe targeting *arcZ* detected the full-length (~132 nt) and processed (~59 nt) transcripts, showing differential accumulation among the allelic variants. 5S rRNA served as a loading control. 3 independent experiments were performed.

Mutations in arcZ are selected rapidly *in planta*

The identified IPO 2222 variants are likely clonally related, differing by only a single-nucleotide mutation across the entire genome, which suggests that the *arcZ* mutants evolved directly from the wild-type strain. To determine the specific conditions driving the selection of these mutations, we

performed experimental evolution assays using the *D. solani* DS624 strain, which carries the functional *arcZ*$_1$ allele and exhibits antifungal activity.

We first investigated the emergence of mutations at the *arcZ* locus under standard laboratory growth conditions. Strain DS624 (*arcZ*$_1$) was passaged four times on LB medium commonly used for *in vitro* experiment. These passages corresponded to approximately 30 bacterial generations. Illumina sequencing of the final populations revealed that the *arcZ* locus remained unaltered, indicating no detectable selective pressure for *arcZ* mutations during typical *in vitro* cultivation (**Table S2**).

In contrast, we investigated evolutionary dynamics within the host by inoculating *D. solani* DS624 into potato tubers. Following an initial 48-hour infection, macerated tissue was collected and used to inoculate fresh tubers for a second passage (**Fig. 2A**). Illumina sequencing of the total bacterial population recovered from infected tubers indicated the presence of polymorphisms at the *arcZ* locus **(Table S2)**. Thus, *in planta* experimental evolution (for a total of ~30 generations) led to the emergence of *arcZ* variants. Given the correlation between ArcZ loss-of-function and reduced antifungal activity, we screened the recovered population for variants displaying a Sol-negative (Sol$^-$) phenotype. From 200 colonies screened per biological replicate (**Fig. 2A**), we identified multiple independent isolates that were unable to inhibit *K. lactis* growth. Whole-genome sequencing (Illumina and Nanopore) combined with targeted Sanger sequencing of the *arcZ* region confirmed that these phenotypes were linked to novel mutations exclusive to the *arcZ* locus. Specifically, we identified a C105T transition (*arcZ*$_4$) in isolate DS932, a G119T transversion (*arcZ*$_5$) in isolate DS944, and a dinucleotide substitution (CT→AA) located 60 nucleotides upstream of *arcZ* transcription start site in the promoter region of isolate DS945 (*arcZ*$_{Pmut}$) (**Fig. 2B & Table 2**). These data indicate that, unlike *in vitro* conditions, the potato tuber environment exerts selective pressure favoring the rapid appearance of *arcZ* loss-of-function mutations.

To confirm the phenotypic impact of these mutations, we assessed the antifungal activity of the evolved variants using a drop test on *K. lactis*-seeded agar **(Fig. 2C**). Consistent with the initial screening, the *arcZ*$_5$ and *arcZ*$_{Pmut}$ variants displayed a Sol-negative phenotype, characterized by the complete absence of an inhibition halo, similar to the *arcZ*$_2$ variant. In contrast, the *arcZ*$_4$ mutant exhibited an intermediate phenotype, producing an inhibition halo that was present but slightly reduced compared to the ancestral *arcZ*$_1$ allele.

We then compared the pathogenicity of the evolved alleles using a potato tuber maceration assay (**Fig. 2D**). Among the evolved variants, the *arcZ*$_5$ mutant phenocopied *arcZ*$_2$, showing a marked reduction in tissue maceration. In contrast, both the *arcZ*$_4$ and *arcZ*$_{Pmut}$ variants retained full virulence, causing disease symptoms comparable to the wild-type *arcZ*$_1$ strain.

Molecular analysis by Northern blot **(Fig. 2E)** and quantification of processed ArcZ amount (**Fig. S2**) provided a basis for these phenotypes **(Fig. 2E)**. The *arcZ*$_5$ strain failed to accumulate the processed sRNA form, mirroring the defect observed in *arcZ*$_2$. This absence of ArcZ explains the simultaneous loss of antifungal activity and virulence in this mutant, suggesting that the G119T mutation compromises sRNA stability. Conversely, both *arcZ*$_4$ and *arcZ*$_{Pmut}$ strains accumulated the processed sRNA. Notably, the *arcZ*$_{Pmut}$ variant, despite being Sol$^-$, produced detectable levels of ArcZ and remained fully virulent. This uncoupling suggests a regulatory hierarchy where solanimycin production requires a high threshold of ArcZ abundance, while virulence functions are maintained even at lower ArcZ concentrations. Furthermore, the *arcZ*$_{Pmut}$ variant provides a critical internal control for the dosage-dependency hypothesis. Because its mutation is located in the promoter region (-60 nt), it produces an ArcZ sRNA with a sequence identical to the wild-type *arcZ*$_1$, albeit at significantly reduced steady-state levels. The fact that this variant, despite producing a structurally native sRNA, selectively loses antimicrobial activity while remaining fully virulent, strongly supports a causal dosage-threshold model rather than a mutation-induced structural artifact.

Finally, to elucidate the drivers behind the rapid *in planta* selection of these mutants, we hypothesized that they might exhibit a higher multiplication rate than the wild-type strain within the host.

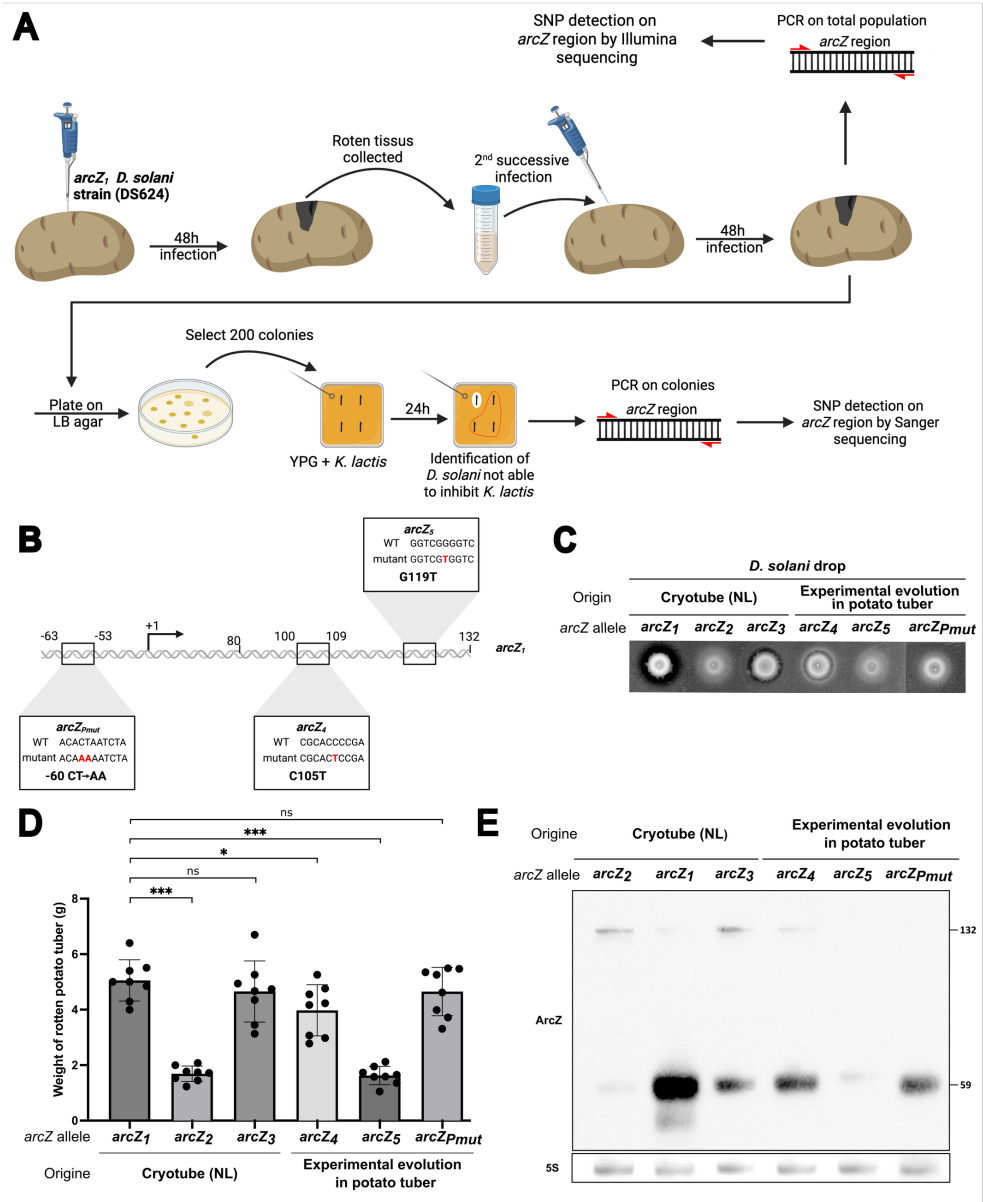

Figure 2. Experimental evolution of *D. solani* in potato tubers reveals novel *arcZ* variants impacting antiyeast activity. (A) Schematic of the experimental evolution assay. The *D. solani* strain DS624 (carrying the *arcZ1* allele) was inoculated into potato tubers. After 48 h, macerated tissue was collected and reinoculated into fresh tubers. Following two infection cycles, bacterial populations were plated on LB agar. Two hundred colonies were screened for the loss of inhibition against *Kluyveromyces lactis* on YPG medium. The *arcZ* region of selected colonies was analyzed by Sanger sequencing, while the total population underwent Illumina sequencing. Pannel made with Biorender. **(B)** Sequence analysis of three novel *arcZ* allelic variants recovered from independent potato infection experiments. The promoter mutant $arcZ_{Pmut}$ contains a dinucleotide substitution (CT→AA) at position –60 relative to the transcription start site. Two variants contain point mutations within the coding sequence: $arcZ_4$ (C105T) and $arcZ_5$ (G119T). **(C)** Antifungal inhibition assays comparing the evolved variants ($arcZ_4$, *arcZ5*, and $arcZ_{Pmut}$) with natural variants from the reference collection ($arcZ_1$, $arcZ_2$). Bacterial cultures were spotted onto *K. lactis*-seeded agar plates and incubated for 48 h at 30 °C (n = 4). **(D)** Virulence of *D. solani arcZ* variants in potato tubers. Tubers were inoculated with standardized bacterial suspensions and incubated for 48 h at 28 °C. Maceration was quantified by weighing the rotten tissue. Evolved variants ($arcZ_4$, $arcZ_5$, $arcZ_{Pmut}$) were compared to ancestral isolates ($arcZ_1$, $arcZ_2$, $arcZ_3$). Data represent the mean ± SD of eight biological replicates (dots). Statistical significance is indicated by asterisks (*** $P < 0.001$, * $P < 0.05$; ns, not significant). **(E)** Northern blot analysis of *arcZ* expression. Total RNA was hybridized with a probe targeting *arcZ*, detecting full-length (~132 nt) and processed (~59 nt) transcripts. 5S rRNA served as a loading control. A representative blot from three independent experiments is shown.

***arcZ* mutants exhibit frequency-dependent competitive fitness in potato tubers**

To determine if *arcZ* loss-of-function variants function as social cheaters, we conducted pairwise competition assays in potato tubers. We competed the wild-type (WT) $arcZ_1$ strain against isogenic mutants carrying derived alleles ($arcZ_2$ through $arcZ_5$) or a promoter mutation ($arcZ_{Pmut}$). Infections were initiated at a 1:100 mutant-to-WT ratio to simulate the emergence of a rare variant. Variants were marked with a gentamicin-resistance (Gm^R) cassette, which imposed no detectable fitness cost **(Fig. S3A)**.
Before assessing competitive fitness, we first quantified the absolute growth of each variant in the host environment when inoculated alone (**Fig. S3B**). We found that the $arcZ_2$ and $arcZ_5$ mutants, which exhibit both reduced virulence and a complete loss of antifungal activity, achieved a significantly lower number of generations in the potato tuber compared to the wild-type $arcZ_1$ strain. However, the $arcZ_4$ and $arcZ_{Pmut}$ variants maintained a proliferation rate similar to the wild-type strain (**Fig. S3B**). This physiological finding aligns with the molecular analysis, which showed that these two variants, $arcZ_4$ and $arcZ_{Pmut}$, produce the highest relative levels of processed ArcZ short form among the tested mutants (**Fig. 2E and Fig. S2**).
Despite these differences in monoculture growth, all *arcZ* variants displayed a significant fitness advantage over the parental strain during co-infection. Following 48 hours, Competitive Indices (CI) ranged from 1.8 to 2.2 (log_{10}), representing a ~100-fold enrichment of the mutant population relative to the initial inoculum (**Fig. 3B**). To confirm that this phenotype is specifically driven by the loss of ArcZ function, we competed a clean deletion mutant $\Delta arcZ_1$ against the WT. The $\Delta arcZ_1$ strain exhibited a high competitive index similar to the natural variants (**Fig. 3B**). Crucially, complementation of the $\Delta arcZ_1$ mutant with a functional $arcZ_1$ copy restored the phenotype to neutral levels (CI ≈ 0), confirming that the lack of ArcZ regulation drives this competitive advantage.
We further investigated the dynamics of this competition through time-course monitoring performed directly on halved potato tubers (**Fig. 3C**). Starting from a 1:100 ratio, the proportion of $\Delta arcZ_1$ mutants increased progressively throughout the infection. Significant enrichment was observed as early as 12 h post-infection ($P < 0.01$) and continued until 48 h, where the mutant fraction approached parity with the WT despite the low initial inoculum.
Finally, to verify if this fitness advantage satisfies the criteria for social cheating, we examined whether the competition outcome was frequency-dependent (**Fig. 3D**). We varied the initial inoculation ratios of $\Delta arcZ_1$ to WT (1:100, 1:1, and 100:1). The fitness gain of the $\Delta arcZ_1$ mutant was inversely proportional to its initial frequency in the population. The mutant showed the highest competitive advantage when rare (1:100), whereas this advantage significantly decreased as the mutant became more common (100:1). This negative frequency-dependent selection is a hallmark of social cheating, suggesting that *arcZ* mutants exploit public goods produced by the $arcZ_1$ wild-type neighbors.

In contrast to the potato tuber environment, no fitness differences were detected under *in vitro* conditions. When grown individually in minimal medium supplemented with sucrose, all *arcZ* variants displayed growth kinetics indistinguishable from the wild-type strain (**Fig. S4A**). Consistently, pairwise competition assays performed in the same *in vitro* medium revealed no significant competitive advantage for the $\Delta arcZ$ mutant (CI ≈ 0) (**Fig. S4B**). These results indicate that the competitive benefit conferred by *arcZ* loss-of-function is strictly context-dependent. This specifically host-driven selection may explain why *arcZ* variants were not detected during experimental evolution in standard laboratory rich medium (**Table S2**).

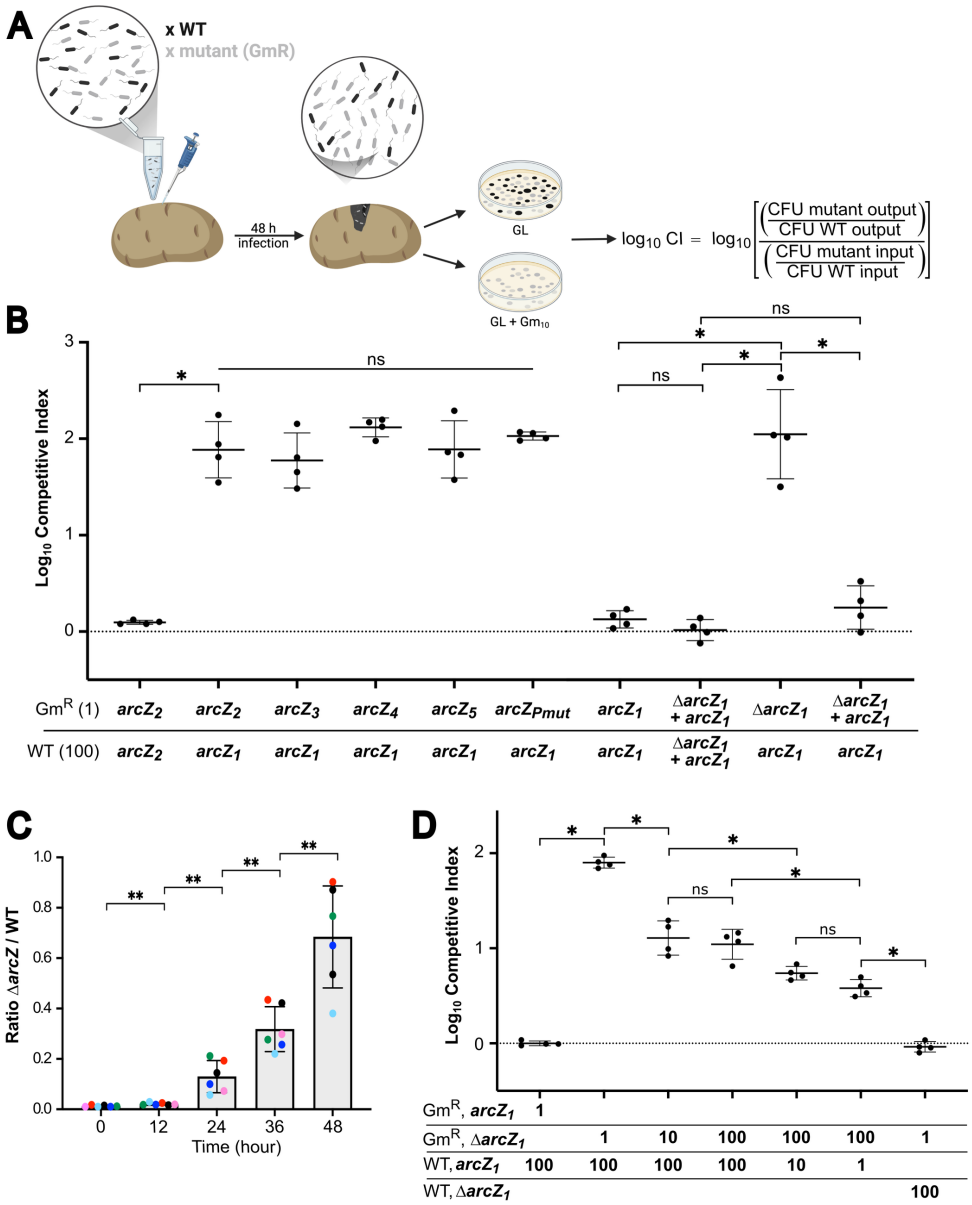

Figure 3. Competitive fitness of *D. solani* strains carrying different *arcZ* mutations during potato infection. **(A)** Schematic representation of the competition assay. Wild-type (WT) and gentamicin-resistant mutant (Gm^R) strains were mixed at defined ratios and inoculated into potato tubers. After 48 h, bacterial populations were recovered and plated on non-selective (GL) and selective (GL + gentamicin) media. The results are expressed as the $\log_{10}$ of the competitive index (CI). **(B)** Competition assays between *arcZ* variants (allelic variants and deletion mutants) and the *arcZ₁* strain. All mutants are gentamicin-resistant and were inoculated at a 1:100 ratio relative to the *arcZ1* strain (total inoculum: 2.10^6 bacteria) in potato tubers. A $\log_{10}$ CI greater than 0 indicates that the mutant outcompetes the *arcZ1* strain. Data represent four independent biological replicates; *, $P < 0.05$; ns, not significant. **(C)** Time-course monitoring of competition dynamics between WT and Δ*arcZ* strains. Tubers were co-infected with a mixture containing 1 Δ*arcZ* to 100 WT bacteria (10^6 bacteria total). At the indicated time points (0 to 48 h post-infection), bacteria were recovered and plated on selective and non-selective media. The ratio of Δ*arcZ* to WT was calculated to assess population dynamics (n=6). **(D)** Effect of initial inoculation frequency on competition outcomes. Competitive assays between WT and Δ*arcZ* strains were performed using different initial ratios (1:100, 100:1, 10:100, 100:10, and 1:1). Bacterial populations were quantified after 48 h of co-infection, and the CI was calculated (n=4).

Evolutionary conservation and predicted structural variation of *arcZ* alleles

To determine the evolutionary context of the adaptive *arcZ* mutations identified in *D. solani*, we analyzed the conservation of the processed ArcZ sequence (short form) across the *Dickeya* genus (**Fig. S5**). Sequence alignment reveals that the substitutions observed in our *D. solani* variants are also

present in other *Dickeya* species. For instance, the G90A substitution, characteristic of the *arcZ*$_2$ allele, is found in several strains of *Dickeya fangzhongdai* (DSM 101847, LN1, QZH3) and *Dickeya parazeae* S31. Similarly, the C105T mutation, which emerged during our experimental evolution assays, exists naturally in *D. fangzhongdai* strain MK7. The recurrence of these specific substitutions suggests that the selection of *arcZ* mutants observed *in planta* is not restricted to *D. solani* but may represent a broader adaptive mechanism across the genus.

To assess the extent of this conservation, we compared the processed ArcZ sequence with representative members of the *Enterobacterales* family. While the *arcZ* seed domain is highly conserved (**Fig. 4A**), the specific residues mutated in *D. solani* (G90A, G101T, C105T, and G119T) correspond to positions that are variable within the family. Notably, the G90A and G101T substitutions align with nucleotides found in the animal pathogens *Salmonella enterica* and *Yersinia pseudotuberculosis*, respectively (**Fig. 4B**). This structural convergence suggests that the instability or processing defects associated with these mutations are likely conserved mechanisms across the *Enterobacterales*.

We used thermodynamic modeling to predict the impact of these substitutions on the folding of the processed sRNA (**Fig. 4C**). The RNAfold algorithm predicts that, while the overall hairpin architecture remains intact, specific mutations induce local conformational shifts. The *arcZ*$_2$ mutation (G90A) disrupts a G–C base pair within the central stem, leading to a widened internal loop compared to the wild-type structure. Similarly, the *arcZ*$_5$ mutation (G119T) is in the 3' region and alters the predicted base-pairing probability of the terminal stem-loop. Interestingly, *arcZ*$_5$ mutations in *Y. pseudotuberculosis* and *Salmonella typhimurium* appear to have the same impact on the secondary structure as in *D. solani* (**Fig. S6A** and **Fig. S6B**). In contrast, the *arcZ*$_3$ (G101T) and *arcZ*$_4$ variants, which displays an intermediate phenotype, possesses a predicted secondary structure nearly identical to the ancestral ArcZ$_1$, with high base-pairing probability throughout the stem. The same pattern was observed for ArcZ$_4$ of *S. typhimurium*. However, the secondary structures of *S. typhimurium* ArcZ$_2$ and ArcZ$_3$ variants appear greatly affected; this disruption is less pronounced in *Y. pseudotuberculosis*, although differences from the ArcZ$_1$ structure remain notable. Collectively, these findings indicate that while the precise structural consequences can vary depending on the genomic context, the targeting of these specific residues represents a recurrent evolutionary pathway for modulating ArcZ function across the *Enterobacterales*.

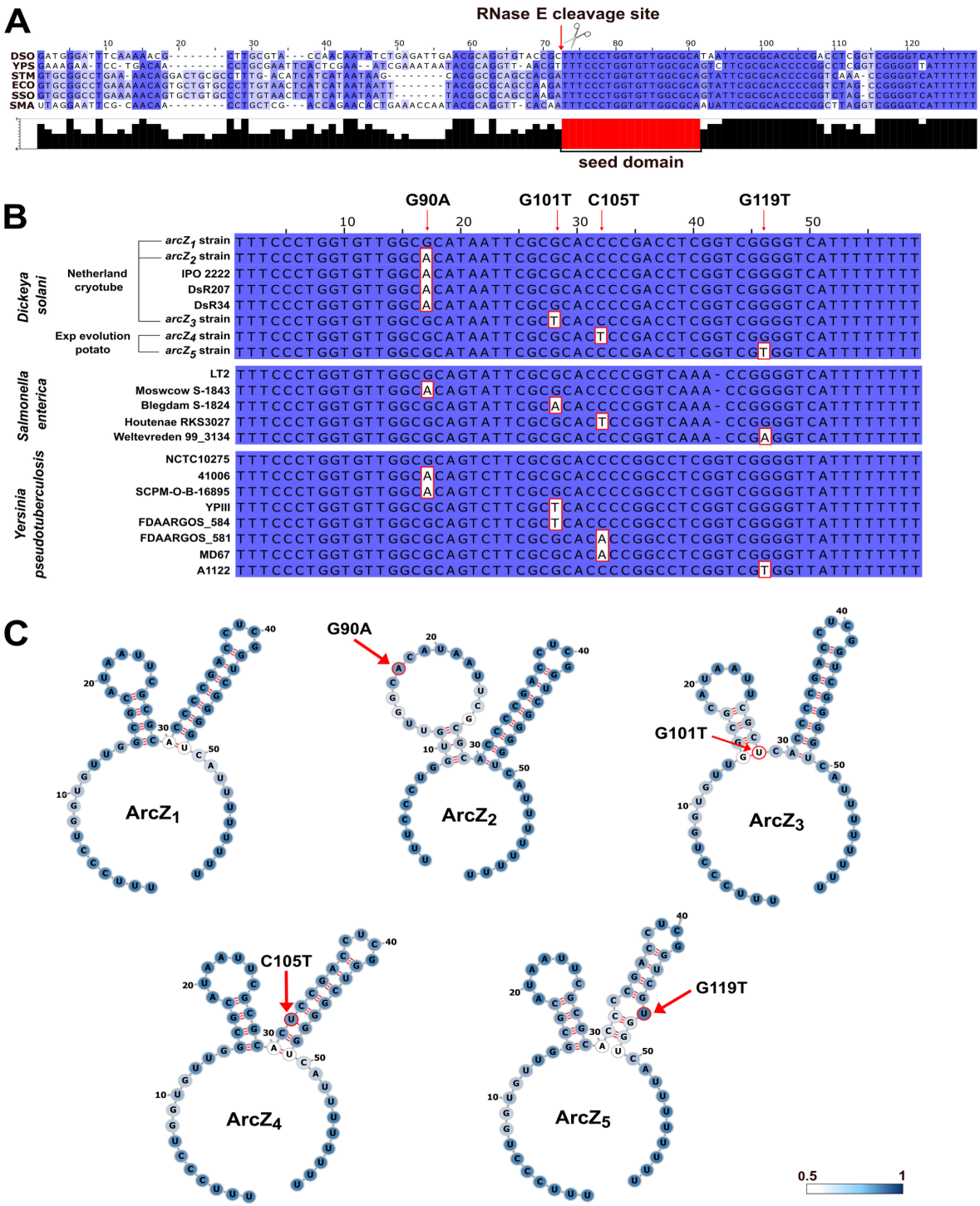

Figure 4. Adaptive *arcZ* mutations identified in *D. solani* are shared with *Salmonella enterica* and *Yersinia pseudotuberculosis* isolates. **(A)** Sequence alignment of ArcZ homologs across representative *Enterobacterales* performed using ClustalW and visualized with Jalview. Nucleotide conservation is indicated in blue, with the conservation scores displayed in the histogram below. The seed domain involved in mRNA pairing is highlighted in red, and the predicted RNase E cleavage site is indicated by an arrow. **(B)** Nucleotide alignment of *arcZ* sequences from *D. solani* isolates, including ancestral cryotube strains ($ArcZ_1$, $ArcZ_2$, and $ArcZ_3$) and evolved variants ($ArcZ_4$ and $ArcZ_5$), compared with *S. enterica* and *Y. pseudotuberculosis* orthologs. Four single-nucleotide substitutions were identified (G90A, G101T, C105T, and G119T); these affect conserved positions within the *arcZ* sequence. **(C)** Predicted secondary structures of the ArcZ RNA variants generated using the RNAfold package. Base-pairing strength is visualized by the number of red connecting lines: three lines denote strong G–C interactions, two lines denote A–U pairs, and one line denotes weak non-canonical interactions. The blue gradient

represents the base-pairing probability predicted by RNAfold, ranging from 0.5 (light blue) to 1 (dark blue). The positions of SNPs (G90A, G101T, C105T, and G119T) are marked by red arrows.

Discussion

Molecular Tuning of Cooperative Traits via sRNA Remodeling

Our study reveals that *Dickeya solani* resolves the physiological trade-off between virulence and secondary metabolism through a rheostat-like modulation of the ArcZ sRNA, rather than a simple binary switch. A central insight from this work is the "uncoupling" of these traits based on intracellular ArcZ dosage. We observe a regulatory hierarchy where virulence functions appear robust, maintained even at low thresholds of processed sRNA, whereas the production of antimicrobial metabolites requires a high concentration of ArcZ. This aligns with the "threshold-linear" model of sRNA regulation (26), where the repression or activation of targets is dynamically defined by the transcription rate and stability of the regulator.

The $arcZ_{Pmut}$ variant provides compelling evidence for this dosage-dependent model. Unlike the coding sequence mutants, $arcZ_{Pmut}$ carries the wild-type $arcZ_1$ allele, with mutations located strictly within the promoter region. This configuration allows for a reduction in transcriptional efficiency, and thus a lower steady-state concentration of the sRNA, without altering the sequence or the predicted secondary structure of the transcript itself. The fact that this variant accumulates intermediate levels of structurally native ArcZ while selectively losing antimicrobial activity, yet remaining fully virulent, strongly supports a causal dosage-threshold mechanism rather than a mutation-induced structural artifact.

While our current results validate the existence of this regulatory hierarchy, defining the precise quantitative requirements for each pathway remains an objective for future study. Utilizing an inducible system to control $ArcZ_1$ titration in a $\Delta arcZ_1$ background will eventually allow us to precisely map the intracellular concentrations required to trigger specific regulated nodes. This approach will confirm whether the observed phenotypic uncoupling is strictly a function of intracellular concentration across all regulated pathways.

Mechanistically, this adaptive modulation is achieved through diverse mutational strategies that target the sRNA's lifecycle. The $arcZ_{Pmut}$ variant, located in the promoter, suggests a reduction in transcriptional efficiency that lowers the steady-state concentration of the sRNA. Conversely, coding sequence mutations likely alter sRNA folding and stability. Structural modeling indicates that the $arcZ_4$ (C105T) mutation disrupts a stable G-C pair in the central stem, potentially impairing Hfq binding (12, 13) or mRNA annealing efficiency without abolishing the transcript entirely. Notably, the specific nucleotides mutated in *D. solani* (e.g., G90, G101) correspond to polymorphic positions in the genomes of *Salmonella* and *Yersinia*. This suggests that these regulatory hotspots represent evolutionarily accessible sites for fine-tuning sRNA activity across *Enterobacterales*, allowing pathogens to rapidly adjust their regulatory networks in response to host pressures.

Rapid Emergence of Social Cheaters and the Hypothesis of Ecological Filtering

The rapid selection of *arcZ* mutants within approximately 30 bacterial generations underscores the intense selective pressure acting on regulatory networks during infection. Our competition assays confirm that these variants behave as conditional social cheaters. They exhibit a negative frequency-dependent fitness advantage, a hallmark of social cheating where rare variants exploit public goods produced by the cooperative majority (3). With a competitive index reaching 100-fold enrichment, these mutants illustrate how "cheating" strategies can rapidly sweep through a population in a nutrient-rich, low-competition environment like the potato tuber.
The selection of "cheater" mutants targeting central regulators appears to be a convergent strategy for optimizing host colonization across diverse pathosystems. For instance, *S.* Typhimurium evolves *hilD*-deficient mutants that cannot colonize independently but outcompete wild-type strains during co-infection by exploiting host inflammation (27). In *Pseudomonas aeruginosa* (5, 28, 29) and *Pseudomonas syringae* (30), non-cooperative variants accumulate by avoiding the metabolic costs associated with quorum sensing or type III secretion systems.

However, our findings distinguish *D. solani* by the molecular nature of the adaptive target. While *Salmonella* and *Pseudomonas* typically select for mutations in proteinaceous regulators, *D. solani* remodels its regulatory network through mutations in a small noncoding RNA. This demonstrates that short noncoding elements can serve as critical, rapidly accessible targets for selection, capable of reshaping microbial social dynamics during infection.

These findings raise critical questions regarding the spatial limits of this selective advantage. We hypothesize that the maintenance of the cooperative wild-type genotype relies on "ecological filtering" driven by the biphasic life cycle of *D. solani*. While the infected tuber favors the proliferation of rapid-growing cheaters, the return to the soil environment likely imposes a different selective regime where the antimicrobial activity regulated by ArcZ becomes essential. Furthermore, the behavior of these variants across the whole plant remains to be defined. It is crucial to verify whether *arcZ* mutants maintain their cheating advantage in other organs, such as stems or leaves, and whether they retain the capacity for systemic dissemination. Future work must determine if these variants can migrate efficiently through vascular tissues or if their rapid selection is a phenomenon restricted to the nutrient-rich niche of the potato tuber.

Defining the Metabolic Currency of Cooperation

While we have established that *arcZ* variants act as social cheaters by exploiting cooperative public goods, the precise metabolic constraint alleviated in these mutants remains to be fully elucidated. The loss of antimicrobial production is the most conspicuous phenotype, yet ArcZ is a pleiotropic regulator known to control a vast post-transcriptional network in related *Enterobacterales*, affecting more than 10% of the genome (13). Consequently, the significant fitness advantage observed *in planta* likely stems from a profound, systemic remodeling of the bacterial transcriptomic and proteomic landscape, rather than the silencing of a single biosynthetic gene cluster.
We hypothesize that the *arcZ* mutants benefit from cumulative metabolic economies across multiple cellular pathways. Testing this hypothesis requires moving beyond single-target analysis to a systems biology approach. Future investigations will need to combine RNA-seq, proteomics, and metabolomics to reconstruct the metabolic fluxes that differentiate "cheaters" from cooperative wild-type strains. Furthermore, determining the exhaustive direct targetome of ArcZ via RIL-seq (RNA interaction by ligation and sequencing) will be essential to map the specific regulatory nodes that govern the trade-off between individual fitness and population-level cooperation.

The Fallacy of the Clonal Reference Strain

Finally, our results demonstrate that the phenotypic discrepancies reported for *D. solani* IPO 2222 (11, 25) arise from active, host-driven evolution rather than passive laboratory drift (31–34). We show that *arcZ* mutations undergo rapid selection during *in planta* infection. Consequently, isolating a single colony from the mixed population of a diseased host carries the risk of selecting a "cheater" mutant rather than the wild-type strain. This process can establish a misleading reference sequence through a founder effect. The presence of multiple variants within the IPO 2222 type stock indicates that the initial recovery likely captured this *in planta* diversity, yet subsequent steps failed to ensure clonal purity. Our finding of pre-existing heterogeneity within the IPO 2222 type stock is supported by both high-depth sequencing and the direct recovery and characterization of the corresponding variants. The concordance between the allele frequencies measured in the total population and the phenotypic screening of 925 individual colonies demonstrates that even low-frequency variants (down to 2%) represent stable, viable sub-populations rather than technical noise. This highlights the critical importance of verifying strain purity immediately after recovery from a host. To avoid such biases, we argue for a paradigm shift that prioritizes assessing post-infection genomic diversity (35) and cross-validating phenotypes across multiple environmental isolates (36), rather than relying on the assumption of clonal homogeneity.

Materials and Methods

Detailed information regarding materials and methods is available in the *SI Appendix*.

Bacterial and fungal strains, plasmids and Oligonucleotides used, and growth conditions

Bacterial strains and plasmids used in this study are listed in **Table S3**. Oligonucleotides used are described in **Table S4**. *Dickeya solani* strains (type strain IPO 2222, GenBank accession no. CP015137.1) were cultivated in Luria-Bertani (LB) broth or M63 minimal medium supplemented with sucrose at 30°C. *Escherichia coli* was grown at 37°C in LB broth. *Kluyveromyces lactis* strain MWL9S1 was grown at 30°C in yeast extract-peptone-glucose (YPD) broth. Antibiotics and supplements were added as required (see *SI Appendix*).

Virulence and Competition Assays

Virulence was assessed using a potato tuber maceration assay. Tubers were inoculated with 2.10^6 bacteria and incubated for 48 hours, after which rotten tissue was weighed. For competition experiments, wild-type and gentamicin-resistant mutant strains were mixed at defined ratios (1:100, 1:1, or 100:1) and inoculated into tubers. Bacterial populations were enumerated on selective and non-selective media to calculate the Competitive Index (CI).

Antimicrobial Activity Assays

Antimicrobial activity was determined by spotting *D. solani* cultures onto YPG agar plates seeded with *K. lactis*. Inhibition halos were visualized after 24 to 48 hours of incubation at 30°C.

Experimental Evolution

In vitro evolution was performed by serially passaging *D. solani* in LB broth for approximately 30 generations. *In host* evolution was conducted by inoculating potato tubers with the $arcZ_1$ strain. After 48 hours (approximately 15 generations), rotten tissue was recovered and used to inoculate fresh tubers for a second passage. After 48 hours of infection, the rot was once again recovered. A PCR on the *arcZ* region was performed and then sent for Illumina sequencing. At the same time, a fraction of the bacterial samples recovered from the infected tissues was spread on plates. After 48 hours, 200 colonies visible on the plates were streaked on YPG medium containing *K. lactis*. After 24 hours of incubation at 30°C, colonies not able to inhibit the growth of *K. lactis* were selected and *arcZ* were sequenced by Sanger sequencing.

RNA Analysis and Sequencing

Total RNA was extracted using the RNAsnap method (37) followed by purification. ArcZ expression was analyzed by Northern blot using the biotinylated probe : AAAAAAAATGACCCCGACCGAGGTCGGGGTGCGCGAATTATGCGCCAACACCAGGGAAAGCG. Whole-genome sequencing (Illumina and Oxford Nanopore) and targeted Sanger sequencing were performed to identify mutations in the *arcZ* locus. The raw NGS datasets are available in https://doi.org/10.6084/m9.figshare.31007098.v1. RNA secondary structures were predicted using RNAfold (38).

RNA Secondary structure prediction

For all ArcZ variants, RNA secondary structures were predicted using the RNAfold algorithm (38). Structural visualizations were generated using the Forna web server (39). Base-pairing interactions were categorized by stability: strong interactions (G-C) are represented by three red lines, medium interactions (A-U) by two red lines, and weak interactions (G-U) by a single line. Base-pairing probabilities are indicated on a color scale ranging from 0.5 (white) to 1.0 (dark blue)

Statistical Analyses.

Statistical analyses were performed using GraphPad Prism software. Differences in maceration weight, bacterial population counts (CFU), and competitive indices (CI) were assessed using the unpaired nonparametric Mann–Whitnseey test. Statistical significance is indicated as follows: *, $P < 0.05$; **, $P < 0.01$; ***, $P < 0.001$; and ****, $P < 0.0001$.

Acknowledgments and Funding Sources

We thank Jan van der Wolf (Wageningen University) for providing the original IPO 2222 cryotube stock. This contribution was essential for investigating the population heterogeneity within the reference strain. We also thank Sonia Humphris (James Hutton Institute) and Robert Czajkowski (University of Gdansk) for providing the IPO 2222 isolates used for the comparative phenotypic and genotypic analyses in this study. This work was supported by the Agence Nationale de la Recherche (grant ANR-22-CE35-0017).

References

1. P. Smith, M. Schuster, Public goods and cheating in microbes. *Current Biology* **29**, R442–R447 (2019).

2. E. A. Rundell, S. A. McKeithen-Mead, B. I. Kazmierczak, Rampant Cheating by Pathogens? *PLOS Pathogens* **12**, e1005792 (2016).

3. M. L. Friesen, Social Evolution and Cheating in Plant Pathogens. *Annual Review of Phytopathology* **58**, 55–75 (2020).

4. R. Popat, *et al.*, Quorum-sensing and cheating in bacterial biofilms. *Proceedings of the Royal Society B: Biological Sciences* **279**, 4765 (2012).

5. K. Czechowska, S. McKeithen-Mead, K. A. Moussawi, B. I. Kazmierczak, Cheating by type 3 secretion system-negative Pseudomonas aeruginosa during pulmonary infection. *Proceedings of the National Academy of Sciences of the United States of America* **111**, 7801 (2014).

6. S. Khayi, P. Blin, T. M. Chong, K.-G. Chan, D. Faure, Complete genome anatomy of the emerging potato pathogen Dickeya solani type strain IPO 2222(T). *Stand Genomic Sci* **11**, 87 (2016).

7. J. M. van der Wolf, *et al.*, Dickeya solani sp. nov., a pectinolytic plant-pathogenic bacterium isolated from potato (Solanum tuberosum). *Int J Syst Evol Microbiol* **64**, 768–774 (2014).

8. J. Mansfield, *et al.*, Top 10 plant pathogenic bacteria in molecular plant pathology. *Molecular plant pathology* **13**, 614–629 (2012).

9. M. A. Matilla, R. E. Monson, G. P. C. Salmond, Dickeya solani. *Trends in Microbiology* **31**, 1085–1086 (2023).

10. F. Van Gijsegem, J. M. van der Wolf, I. K. Toth, Eds., *Plant Diseases Caused by Dickeya and Pectobacterium Species* (Springer International Publishing, 2021).

11. T. Brual, *et al.*, A natural single nucleotide mutation in the small regulatory RNA ArcZ of Dickeya solani switches off the antimicrobial activities against yeast and bacteria. *PLOS Genetics* **19**, e1010725 (2023).

12. K. Papenfort, *et al.*, Specific and pleiotropic patterns of mRNA regulation by ArcZ, a conserved, Hfq-dependent small RNA. *Molecular Microbiology* **74**, 139–158 (2009).

13. Q. Dubois, *et al.*, Function and mechanism of action of the small regulatory RNA ArcZ in Enterobacterales. *RNA* **30**, 1107–1121 (2024).

14. Y. Chao, *et al.*, In Vivo Cleavage Map Illuminates the Central Role of RNase E in Coding and Non-coding RNA Pathways. *Mol Cell* **65**, 39–51 (2017).

15. P. Mandin, S. Gottesman, Integrating anaerobic/aerobic sensing and the general stress response through the ArcZ small RNA. *EMBO J* **29**, 3094–3107 (2010).

16. N. De Lay, S. Gottesman, A complex network of small non-coding RNAs regulate motility in Escherichia coli. *Molecular Microbiology* **86**, 524–538 (2012).

17. X. Yuan, *et al.*, A feed-forward signalling circuit controls bacterial virulence through linking cyclic di-GMP and two mechanistically distinct sRNAs, ArcZ and RsmB. *Environmental Microbiology* **21**, 2755–2771 (2019).

18. F. Van Gijsegem, P. Portier, G. Taghouti, J. Pédron, Clonality and Diversity in the Soft Rot Dickeya solani Phytopathogen. *IJMS* **24**, 17553 (2023).

19. M. Golanowska, *et al.*, Comparison of Highly and Weakly Virulent Dickeya solani Strains, With a View on the Pangenome and Panregulon of This Species. *Front Microbiol* **9**, 1940 (2018).

20. J. Fikowicz-Krosko, R. Czajkowski, Systemic Colonization and Expression of Disease Symptoms on Bittersweet Nightshade (Solanum dulcamara) Infected with a GFP-Tagged Dickeya solani IPO2222 (IPO2254). *Plant Dis* **102**, 619–627 (2018).

21. W. Lisicka, *et al.*, Oxygen Availability Influences Expression of Dickeya solani Genes Associated With Virulence in Potato (Solanum tuberosum L.) and Chicory (Cichorium intybus L.). *Front Plant Sci* **9**, 374 (2018).

22. R. Czajkowski, *et al.*, Genome-Wide Identification of Dickeya solani Transcriptional Units Up-Regulated in Response to Plant Tissues From a Crop-Host Solanum tuberosum and a Weed-Host Solanum dulcamara. *Front Plant Sci* **11**, 580330 (2020).

23. D. Figaj, *et al.*, Lon Protease Is Important for Growth Under Stressful Conditions and Pathogenicity of the Phytopathogen, Bacterium Dickeya solani. *Int J Mol Sci* **21** (2020).

24. P. Blin, *et al.*, Pattern and causes of the establishment of the invasive bacterial potato pathogen Dickeya solani and of the maintenance of the resident pathogen D. dianthicola. *Molecular Ecology* **30**, 608–624 (2021).

25. M. A. Matilla, *et al.*, Solanimycin: Biosynthesis and Distribution of a New Antifungal Antibiotic Regulated by Two Quorum-Sensing Systems. *mBio* e02472-22 (2022). https://doi.org/10.1128/mbio.02472-22.

26. E. Levine, T. Hwa, Small RNAs establish gene expression thresholds. *Current Opinion in Microbiology* **11**, 574–579 (2008).

27. M. Diard, *et al.*, Stabilization of cooperative virulence by the expression of an avirulent phenotype. *Nature* **494**, 353–356 (2013).

28. K. M. Sandoz, S. M. Mitzimberg, M. Schuster, Social cheating in Pseudomonas aeruginosa quorum sensing. *Proceedings of the National Academy of Sciences* **104**, 15876–15881 (2007).

29. K. Zhao, *et al.*, Evolution of lasR mutants in polymorphic Pseudomonas aeruginosa populations facilitates chronic infection of the lung. *Nat Commun* **14**, 5976 (2023).

30. T. Xie, *et al.*, Natural variation in the hrpL promoter renders the phytopathogen Pseudomonas syringae pv. actinidiae nonpathogenic. *Molecular Plant Pathology* **24**, 262–271 (2023).

31. I. Artuso, *et al.*, Genome diversity of domesticated Acinetobacter baumannii ATCC 19606T strains. *Microb Genom* **8**, 000749 (2022).

32. L. C. Jacques, *et al.*, Influence of Streptococcus pneumoniae Within-Strain Population Diversity on Virulence and Pathogenesis. *Microbiol Spectr* **11**, e03103-22.

33. B. Spira, R. de Almeida Toledo, R. P. Maharjan, T. Ferenci, The uncertain consequences of transferring bacterial strains between laboratories - rpoS instability as an example. *BMC Microbiol* **11**, 248 (2011).

34. J. Klockgether, *et al.*, Genome Diversity of Pseudomonas aeruginosa PAO1 Laboratory Strains. *Journal of Bacteriology* **192**, 1113–1121 (2010).

35. Appendix R: Guidelines for Verifying and Documenting the Relationships Between Microbial Cultures. *J AOAC Int* **103**, 900–903 (2020).

36. J. Nysten, D. Sofras, P. Van Dijck, One species, many faces: The underappreciated importance of strain diversity. *PLoS Pathog* **20**, e1011931 (2024).

37. M. B. Stead, *et al.*, RNA snap ™: a rapid, quantitative and inexpensive, method for isolating total RNA from bacteria. *Nucleic Acids Research* **40**, e156–e156 (2012).

38. I. L. Hofacker, *et al.*, Fast folding and comparison of RNA secondary structures. *Monatsh Chem* **125**, 167–188 (1994).

39. P. Kerpedjiev, S. Hammer, I. L. Hofacker, Forna (force-directed RNA): Simple and effective online RNA secondary structure diagrams. *Bioinformatics* **31**, 3377–3379 (2015).

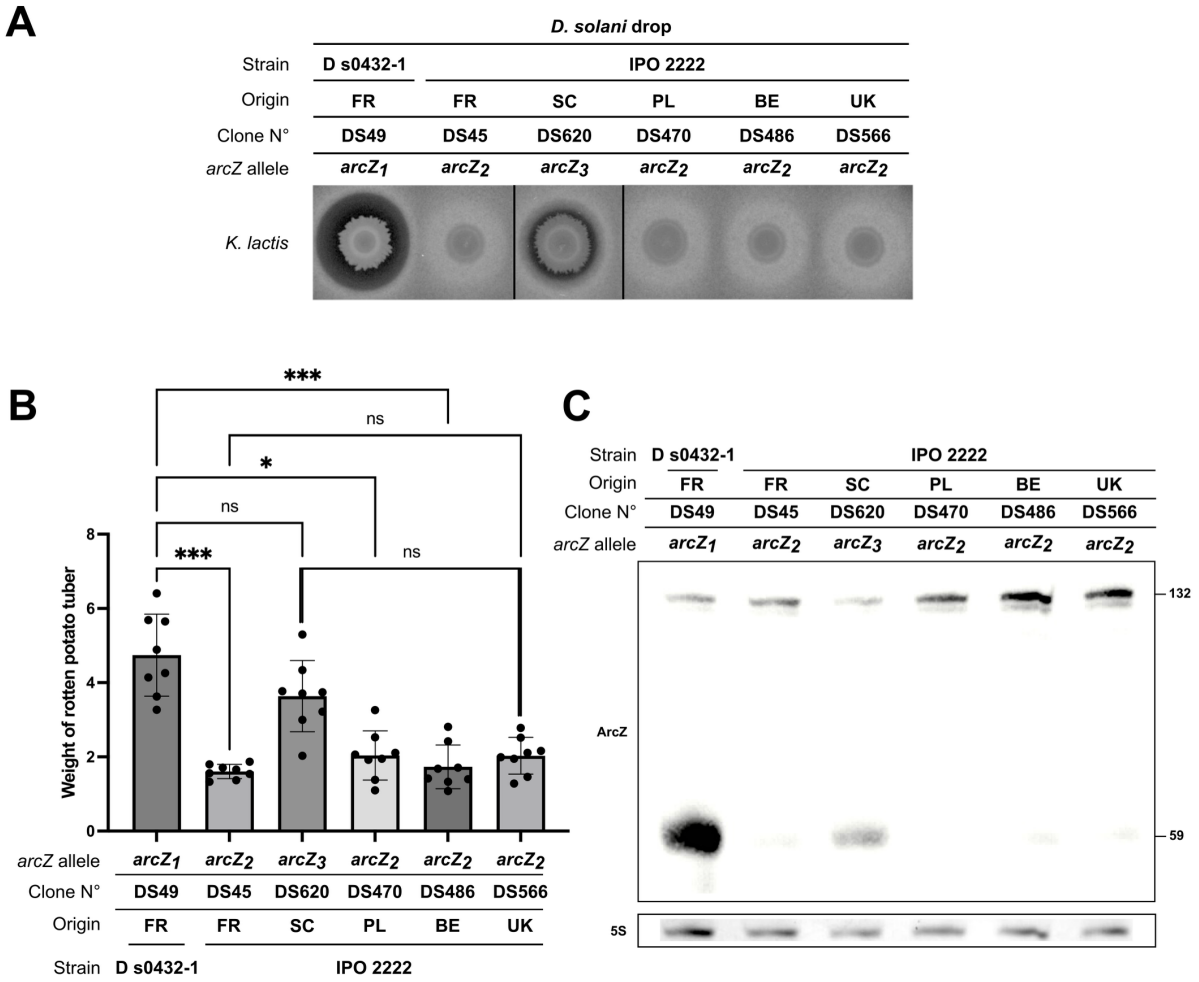

Figure S1. Phenotypic and molecular characterization of European *D. solani* isolates carrying distinct *arcZ* alleles. (A) Antifungal activity against *Kluyveromyces lactis*. Bacterial cultures of D. solani from different country were spotted on yeast-containing agar plates and incubated for 48 h at 28 °C (FR = France, IPO 2222 DS45, SC = Scotland IPO 2222 DS620, PL = Poland IPO 2222 DS470, BE = Belgium IPO 2222 DS486, UK = United Kingdom IPO 2222 DS566). Representative images of inhibition halos are shown (n = 4). **(B)** Virulence quantification on potato tubers. Maceration was assessed by measuring the weight of rotten tissue per tuber after 48 h of incubation at 28 °C. Data represent mean ± SD (n = 8). Statistical significance was determined using one-way ANOVA followed by Tukey's post hoc test (***P < 0.001; *P < 0.05; ns, not significant). **(C)** Northern blot analysis of *arcZ* expression. A probe targeting *arcZ* detected two RNA species (~132 nt and ~59 nt). 5S rRNA served as a loading control. Representative blot from three independent experiments is shown.

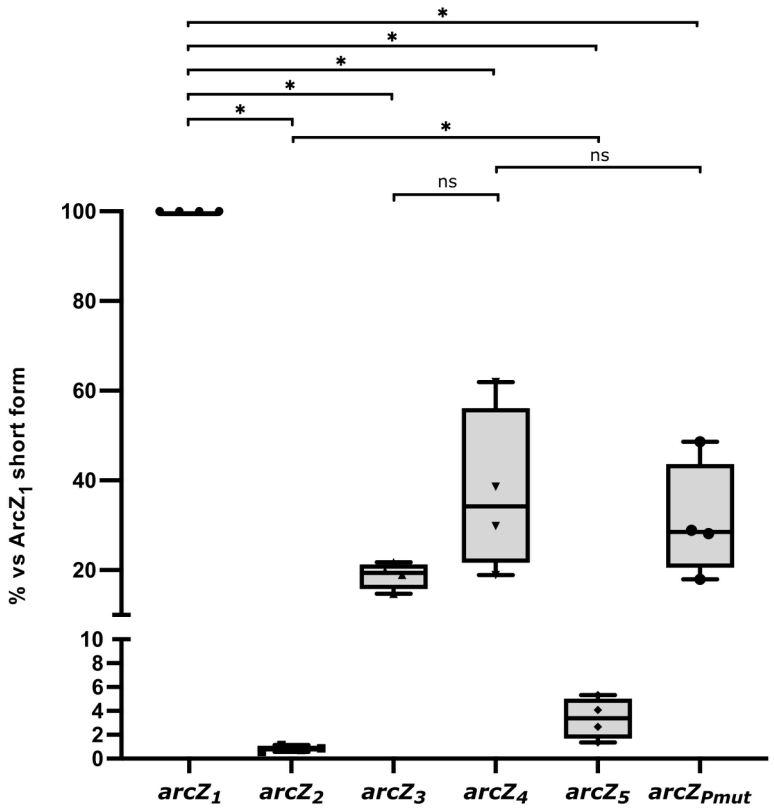

Figure S2. Quantification of processed ArcZ RNA abundance. The relative levels of the short ArcZ transcript (~59 nt) were determined by densitometry of Northern blots. Signal intensities were normalized to 5S rRNA and expressed as a percentage of the *arcZ1* reference strain (set to 100%). Box plots show the distribution of four independent biological replicates. Statistical significance was determined using the Mann-Whitney test ($P < 0.05$; ns, not significant).

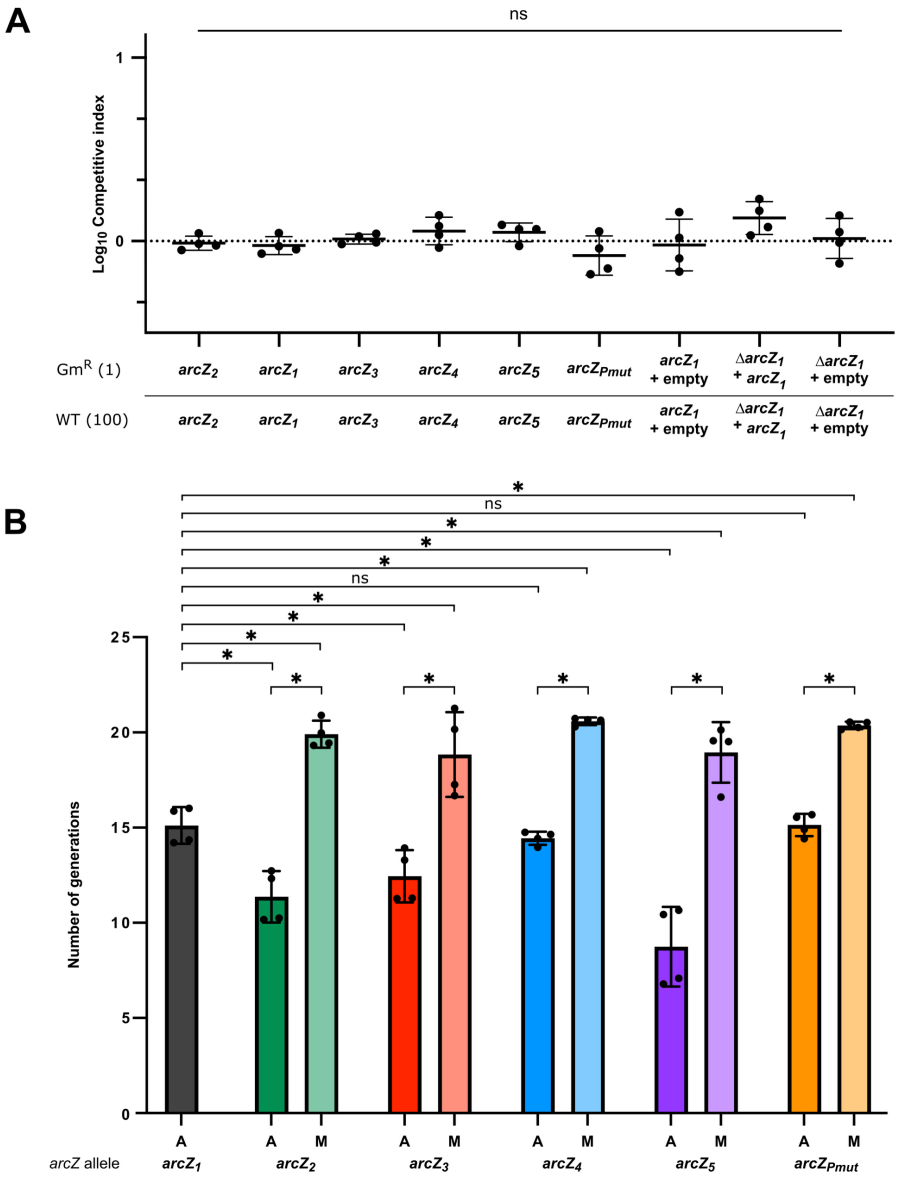

Figure S3. Control assays for fitness and growth dynamics of *D. solani arcZ* variants in potato tubers. (A) Assessment of the gentamicin resistance marker cost. Strains carrying specific *arcZ* alleles were coinoculated with their isogenic unlabeled counterparts (1:100 ratio) in potato tubers. The Log_{10} Competitive Index (CI) was determined after 48 h. Values near zero indicate that the marker imposes no detectable fitness cost. **(B)** Bacterial proliferation in single versus mixed infections. The number of generations was calculated for strains inoculated either alone (A) or mixed with the *arcZ*$_1$ reference strain (M). Data were derived from CFU counts after 48 h. Bars represent mean ± SD of independent biological replicates. Statistical significance was determined ;$P < 0.05$; ns, not significant).

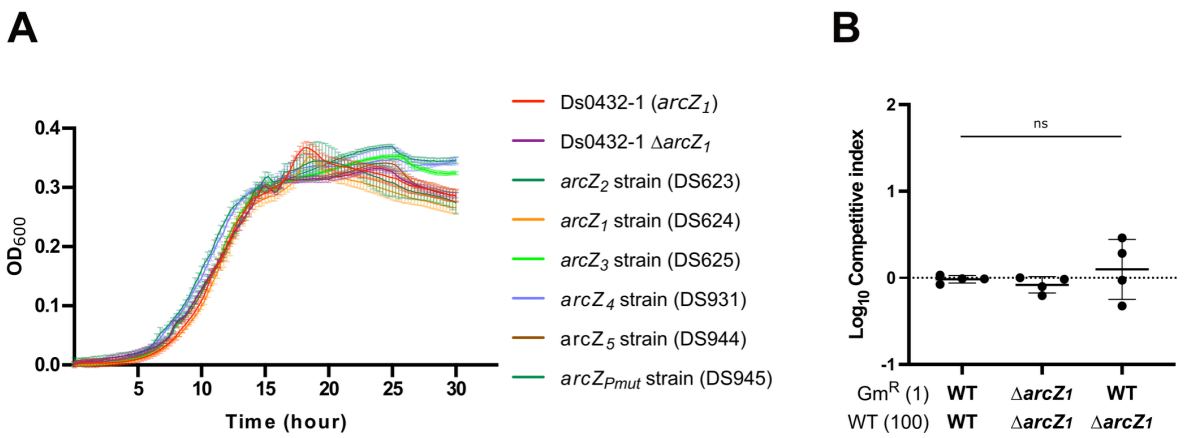

Figure S4. *In vitro* growth kinetics of *D. solani* strains and mutants and competition assay *in vitro*. (A) Cultures were grown in M63 minimal medium supplemented with 1% sucrose at 30°C. Strains were inoculated into 96-well plates at an initial OD_{600} of 0.06. Optical density was monitored every 15 min for 30 h using a microplate reader. Data represent mean ± SD. Statistical analysis indicated similar growth profiles across all strains (Mann-Whitney test; $P > 0.05$). (B) Competition assays between Δ*arcZ* and the WT strain. Mutants correspond to gentamicin-resistant strains and were inoculated at a 1:100 ratio relative to the WT (total inoculum: 2.10^6 bacteria) in potato tubers. A $\log_{10}$ CI greater than 0 indicates that the mutant outcompetes the WT strain. Data represent four independent biological replicates; *, $P < 0.05$; ns, not significant.

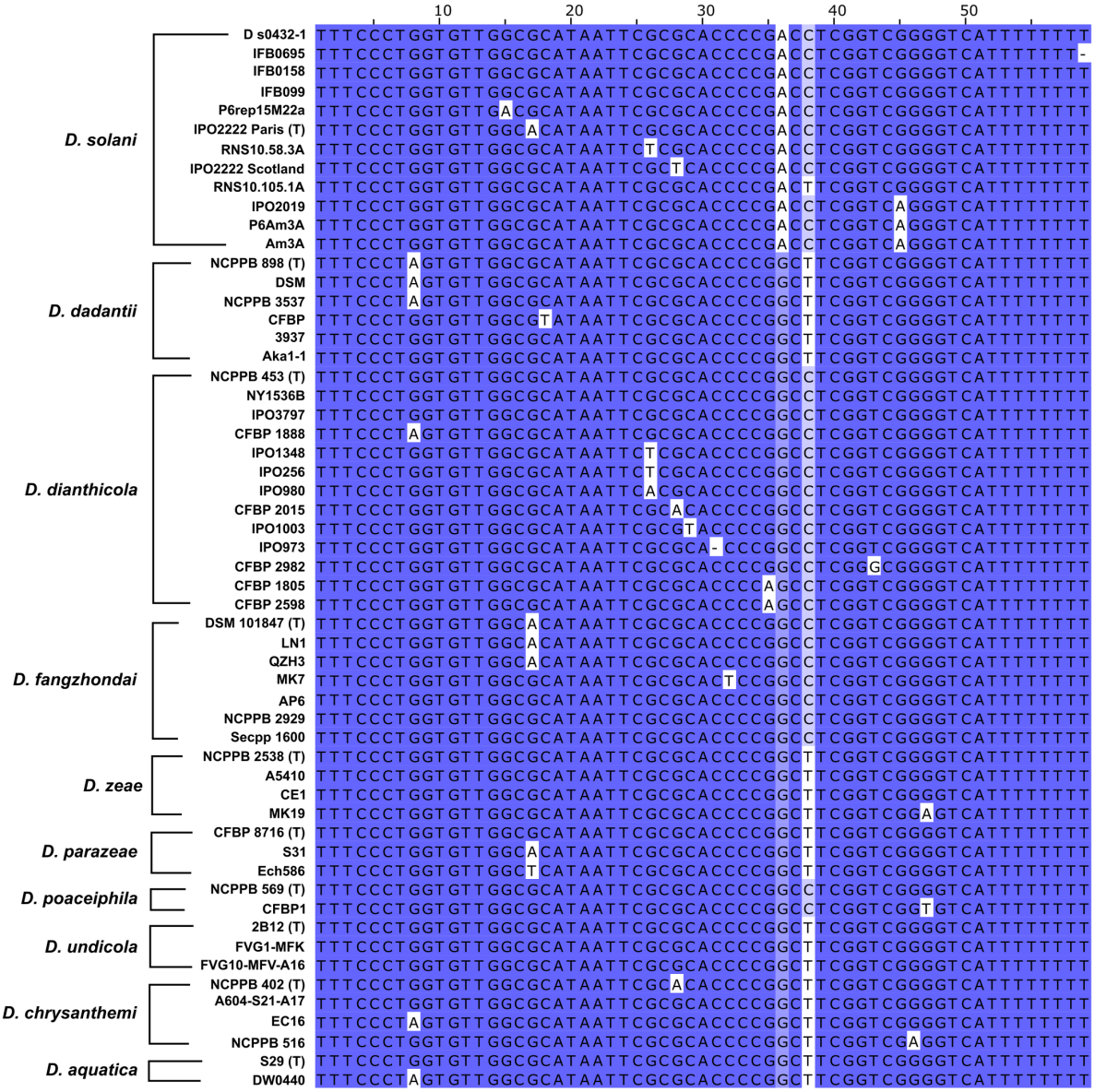

Figure S5. Conservation of the processed *arcZ* sequence across the *Dickeya* genus. Multiple sequence alignment of the *arcZ* genomic region encoding the short RNA form (~59 nt) from representative strains of ten *Dickeya* species. For each species group, the reference wild-type (WT) sequence is listed first. Dark blue shading denotes nucleotide identity, while white backgrounds indicate polymorphic positions. The alignment was generated using ClustalW and visualized with Jalview.

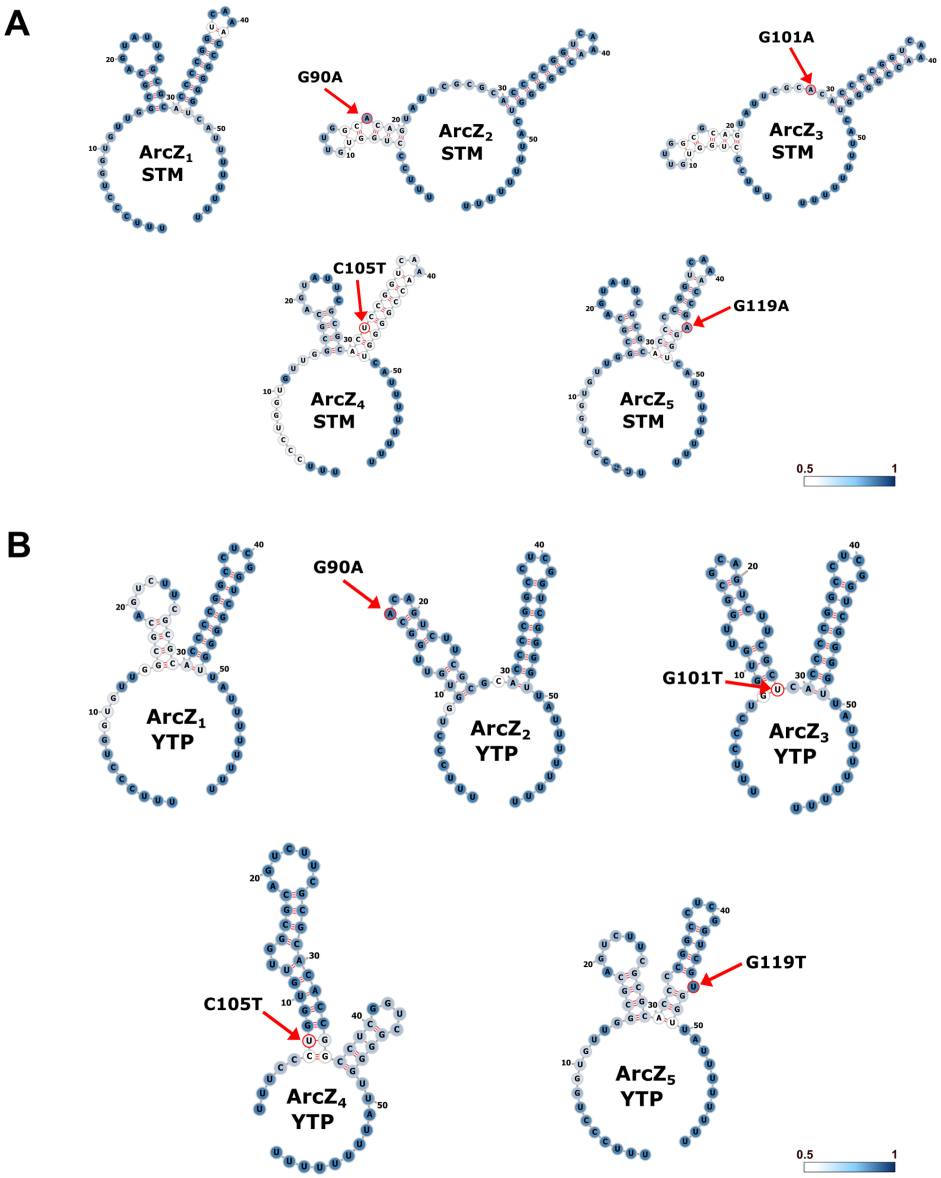

Figure S6. Predicted secondary structures of *ArcZ* variants in *Salmonella enterica* and *Yersinia pseudotuberculosis*. (A) *S. enterica* (STM) structures modeled with substitutions identified in *D. solani* (G90A, G101A, C105T, and G119A). **(B)** *Y. pseudotuberculosis* (YTP) structures carrying analogous substitutions (G90A, G101T, C105T, and G119T). Secondary structures were predicted using the ViennaRNA package (RNAfold). Red arrows indicate the positions of single-nucleotide substitutions. The color gradient reflects base-pairing probability, ranging from 0.5 (light blue) to 1.0 (dark blue).